ISSN 1392 - 1207. MECHANIKA. 2005. Nr.5(55)

Multilayer tubular composite reinforced by a liner: behaviour under pressure loading simulation

A. Hocine*, A. Bezazi, L. Boubakar***, A. Benamar****, A. Kondratas*****

*University Hassiba Benbouali of Chlef BP. 151, 02000 Chlef, Algeria, E-mail: Hocinea_dz@Yahoo.fr

**University 08 Mai 1945, BP. 401, 24000 Guelma, Algeria, E-mail: ar_bezazi@yahoo.com

***University of Franche-Comté, LMARC, 24, chemin de l'Epitaphe, 25000 Besançon, France, E-mail: lamine.boubakar@univ-fcomte.fr

****ENSET, Department of mechanical engineering, BP 1523, 31000 Oran, Algeria, E-mail: benamar_dz@yahoo.fr

*****Kaunas University of Technology, Donelaicio str. 73, 44029 Kaunas, Lithuania, E-mail: Alvydas.Kondratas@ktu.lt

1. Introduction

The use of composite materials is an extremely interesting alternative to metallic materials in the construction of tanks. Indeed, these materials are characterized by their lightness, rigidity, good fatigue strength, and corrosion resistance when their components are not metallic [1-3]. Very fast increases in demands for composite materials in various civil and military industrial applications consider the advantages especially in the design of tanks. Thin or thick walled tanks are widely used in several branches of engineering, such as: the storage of compressed hydrogen, liquefied, and compressed natural gas [4, 5]. The multi-layer tanks are ideal for the structure under static and dynamic loading. The rolling up filament is an effective method for the manufacture of multilayer composite tanks. The obtained structures find broad applications when they are subjected to internal/external pressure, flexure, torsion, and axial loading [6]. This technique is also adopted for the tanks with high pressure for the storage of oxygen and fuel, etc.

Beneficial composite tank can be achieved by adapted design, good rigidity of the tank and pre-stresses optimisation. A multilayer tank, under high pressure must resist to the maximum service pressure, as well as to the fatigue loading cycles, which result from the cycle charges discharge. Rupture of the first layer is considered as total rupture of the tank in the design of unidirectional layer tanks, moreover then the permeability problem acquires [6-7]. However, when the tank is designed with different layer orientations, rupture of the first layer is not necessarily the total rupture of the tank [7]. In order to remediate gases leakage problem, the filaments are coated on a metal liner. This new model of storage is regarded as a hybrid structure, where the liner provides the sealing and the corrosion resistance while rolling up is charged to resist to the high internal pressures as well as resist to the tension loading. Hybrid approach ensures perfect participation between the liner and the composite hull. Weight saving that can be achieved with load-bearing metal liner reinforced with composite over wrap, compared to all metal vessels, is about 50% [7].

The study of the stress and strain reveals a significant key in the design and the choice of the tanks. Several researches have challenged to optimise the stacking sequence of the composite structure. The analytical procedure has been used to determine the stress and the strain of a cylindrical structure under various loading conditions [6]. It challenges the determination of adequate stacking sequence in order to improve the resistance of the Glass Fibber Reinforced Polymer (GFRP) cylindrical composite tanks [8]. Numerical model of the structure using "Blocks" and SAP90 software has been used to determine the stress and strain fields. Stress and strain of a laminate composite tube has been determined using the classical laminates theory and varying the fibre orientation angle between 15° and 85° [9]. This shows that the angle of 55° is optimum for a tube in filament rolling-up with a stress ratio of circumferential/axial of 2:1, and in the case of a tube under the pressure, without axial loading, the optimum angle is of 75°. It can be concluded that the ratio of circumferential/axial stress varies according to the type of stacking sequence for the cylindrical containers with different orientation angles of the composite layers [10, 11].

The aim of this work consists of the analysis of stress and strain of a multi-layer composite tube coated by a metal liner. The objective is to determine the adequate stacking sequence in order to improve the resistance of the cylindrical composite tanks under external and internal pressures. This study is undertaken on two types of stacking sequences: the multilayer anti-symmetric ($\pm\varphi_{2n}$) and the quasi-isotropic laminate ($\pm\varphi_n/90_{2n}$).

2. Analysis procedure

2.1. Stress and strain analysis

The stress and strain analysis of a cylindrical composite tube of internal and external radius r_0, r_a respectively subjected to an axisymmetric internal pressure loading p_0 is processed. Cylindrical coordinates are useful in analyzing surfaces that are symmetrical about an axis with the z axis chosen as the axis of symmetry. The cylindrical composite tube has been placed in the cylindrical coordinate system for the analysis and modelling of the behaviour, where the cylinder coordinates are defined: r radial, θ circumferential, and z axial coordinates of the cylinder (Fig. 1). Stresses and strains are independent of θ due to the axisymetric loading. In addition, radial and axial displacements depend only on z and r respectively. Thus, the field of displacement is [10, 11]

$$\begin{cases} U_r = U_r(r) \\ U_\theta = U_\theta(r,z) \\ U_z = U_z(z) \end{cases} \tag{1}$$

where U_r, U_θ , and U_z are radial, circumferential, and axial displacements respectively.

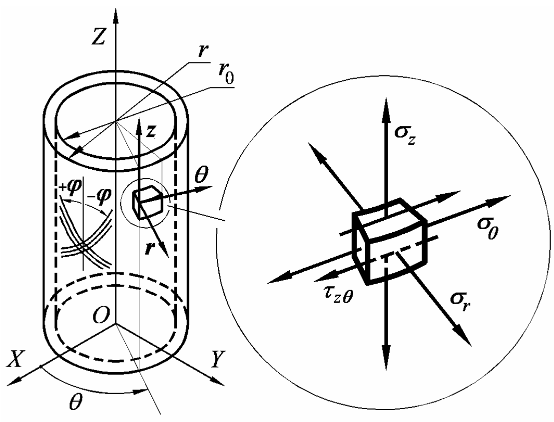

Fig. 1 Stress state of in a multi-layer tube

The stress/strain relations of the k th layer of anisotropic materials can be given by

$$\begin{Bmatrix} \boldsymbol{\sigma}_z \\ \boldsymbol{\sigma}_\theta \\ \boldsymbol{\sigma}_r \\ \boldsymbol{\tau}_{\theta r} \\ \boldsymbol{\tau}_{zr} \\ \boldsymbol{\tau}_{z\theta} \end{Bmatrix}^{(k)} = \begin{bmatrix} \boldsymbol{C}_{11} & \boldsymbol{C}_{12} & \boldsymbol{C}_{13} & 0 & 0 & \boldsymbol{C}_{16} \\ \boldsymbol{C}_{12} & \boldsymbol{C}_{22} & \boldsymbol{C}_{23} & 0 & 0 & \boldsymbol{C}_{26} \\ \boldsymbol{C}_{13} & \boldsymbol{C}_{23} & \boldsymbol{C}_{33} & 0 & 0 & \boldsymbol{C}_{36} \\ 0 & 0 & 0 & \boldsymbol{C}_{44} & \boldsymbol{C}_{45} & 0 \\ 0 & 0 & 0 & \boldsymbol{C}_{45} & \boldsymbol{C}_{55} & 0 \\ \boldsymbol{C}_{16} & \boldsymbol{C}_{26} & \boldsymbol{C}_{36} & 0 & 0 & \boldsymbol{C}_{66} \end{bmatrix}^{(k)} \begin{Bmatrix} \varepsilon_z \\ \varepsilon_\theta \\ \varepsilon_r \\ \gamma_{\theta r} \\ \gamma_{zr} \\ \gamma_{z\theta} \end{Bmatrix}^{(k)} \quad (2)$$

where $\boldsymbol{\sigma}_z$, $\boldsymbol{\sigma}_\theta$, and $\boldsymbol{\sigma}_r$ are axial, circumferential, and radial stress vectors respectively; $\boldsymbol{\tau}_{z\theta}$, $\boldsymbol{\tau}_{zr}$, and $\boldsymbol{\tau}_{\theta r}$ are shear strain vectors in the plans z-θ, z-r, θ-r respectively; k is the number of the respective layer; $\boldsymbol{C}_{11}$-$\boldsymbol{C}_{66}$ are rigidity coefficients of the respective layer, $\boldsymbol{\varepsilon}_z$, $\boldsymbol{\varepsilon}_\theta$, and $\boldsymbol{\varepsilon}_r$ are axial, circumferential, and radial strain vectors respectively; $\boldsymbol{\gamma}_{\theta r}$, $\boldsymbol{\gamma}_{zr}$, and $\boldsymbol{\gamma}_{z\theta}$ are the shear strain vector in the plan θ-r, z-r , and z-θ respectively.

The strain/displacement relations for the k th layer can be written as follows

$$\varepsilon_r^{(k)} = \frac{\partial U_r^{(k)}}{\partial r};\ \varepsilon_\theta^{(k)} = \frac{1}{r}\frac{\partial U_\theta^{(k)}}{\partial \theta} + \frac{U_r^{(k)}}{r};\ \varepsilon_z^{(k)} = \frac{\partial U_z^{(k)}}{\partial z} \quad (3a)$$

$$\gamma_{z\theta}^{(k)} = \frac{1}{r}\frac{\partial U_z^{(k)}}{\partial \theta} + \frac{\partial U_\theta^{(k)}}{\partial z} \quad (3b)$$

$$\gamma_{zr}^{(k)} = \frac{\partial U_z^{(k)}}{\partial r} + \frac{\partial U_r^{(k)}}{\partial z} \quad (3c)$$

$$\gamma_{\theta r}^{(k)} = \frac{1}{r}\frac{\partial U_r^{(k)}}{\partial \theta} + r\frac{\partial}{\partial r}\left(\frac{U_\theta^{(k)}}{r}\right) \quad (3d)$$

where $\varepsilon_r^{(k)}$, $\varepsilon_\theta^{(k)}$, $\varepsilon_z^{(k)}$ are radial, circumferential, and axial strain vectors of the k th layer respectively; $\gamma_{z\theta}^{(k)}$, $\gamma_{zr}^{(k)}$, $\gamma_{\theta r}^{(k)}$ are shear strain vectors in the planes z-θ, z-r, θ-r respectively; $U_r^{(k)}$, $U_\theta^{(k)}$, $U_z^{(k)}$ are radial, circumferential, and axial displacements of the k th layer respectively.

As for the equilibrium equations in cylindrical coordinates, they take the following form [12]

$$\frac{\partial \sigma_r^{(k)}}{\partial r} + \frac{1}{r}\frac{\partial \tau_{\theta r}^{(k)}}{\partial \theta} + \frac{\partial \tau_{zr}^{(k)}}{\partial z} + \frac{\sigma_r^{(k)} - \sigma_\theta^{(k)}}{r} = 0 \quad (4a)$$

$$\frac{\partial \tau_{\theta r}^{(k)}}{\partial r} + \frac{1}{r}\frac{\partial \sigma_\theta^{(k)}}{\partial \theta} + \frac{\partial \tau_{z\theta}^{(k)}}{\partial z} + \frac{2\tau_{\theta r}^{(k)}}{r} = 0 \quad (4b)$$

$$\frac{\partial \tau_{zr}^{(k)}}{\partial r} + \frac{1}{r}\frac{\partial \tau_{z\theta}^{(k)}}{\partial \theta} + \frac{\partial \sigma_z^{(k)}}{\partial z} + \frac{\tau_{zr}^{(k)}}{r} = 0 \quad (4c)$$

where $\sigma_r^{(k)}$, $\sigma_\theta^{(k)}$, $\sigma_z^{(k)}$ are radial, circumferential, and axial stress vectors of the k th layer respectively; $\tau_{z\theta}^{(k)}$, $\tau_{zr}^{(k)}$, $\tau_{\theta r}^{(k)}$ are shear stress in the plane z-θ, z-r, and θ-r of the k th layer respectively.

The axisymmetric loading of the multi-layer tube allows to reduce equations (4) according to the following context: $\left(\frac{\partial \sigma_{ij}}{\partial \theta} = 0, \frac{\partial \sigma_{ij}}{\partial z} = 0\right)$ [12]. In this case the second and the third terms of the equations (4 a, b, c) are negligible and can be expressed as

$$\frac{d\sigma_r^{(k)}}{dr} + \frac{\sigma_r^{(k)} - \sigma_\theta^{(k)}}{r} = 0 \quad (5a)$$

$$\frac{d\tau_{\theta r}^{(k)}}{dr} + \frac{2}{r}\tau_{\theta r}^{(k)} = 0 \quad (5b)$$

$$\frac{d\tau_{zr}^{(k)}}{dr} + \frac{\tau_{zr}^{(k)}}{r} = 0 \quad (5c)$$

Strain/displacement relations can be also reduced as

$$\varepsilon_r^{(k)} = \frac{dU_r^{(k)}}{dr};\ \varepsilon_\theta^{(k)} = \frac{U_r^{(k)}}{r};\ \varepsilon_z^{(k)} = \frac{dU_z^{(k)}}{dz} = \varepsilon_0 \quad (6a)$$

$$\gamma_{zr}^{(k)} = 0;\ \gamma_{\theta r}^{(k)} = \frac{dU_\theta^{(k)}}{dr} - \frac{U_\theta^{(k)}}{r};\ \gamma_{z\theta}^{(k)} = \frac{dU_\theta^{(k)}}{dz} = \gamma_0 r \quad (6b)$$

where γ_0 has physical interpretation - twist of the pipe per unit length.

These relations are based on the hypothesis that axial strains of all layers are equal to a constant ε_0, i.e. $\varepsilon_z = \varepsilon_0$ and that rotation of the cylinder $\gamma_{z\theta}$ is independent of z [10].

The two equations (5b) and (5c) can be solved according to the following form

$$\tau_{\theta r}^{(k)} = \frac{A^{(k)}}{r^2};\quad \tau_{zr}^{(k)} = \frac{B^{(k)}}{r} \quad (7)$$

where $A^{(k)}$ and $B^{(k)}$ are integration constants of equations (5b) and (5c).

2.2. Behaviour of the metal liner

Isotropic character of the thick metal (aluminium) liner behaviour, permits to write the elastic tensor of rigidity in the cylindrical reference coordinates of the tank in the following form [12, 13]

$$\boldsymbol{C}_l = \begin{bmatrix} \boldsymbol{C}_{11} & \boldsymbol{C}_{12} & \boldsymbol{C}_{12} & 0 & 0 & 0 \\ \boldsymbol{C}_{12} & \boldsymbol{C}_{11} & \boldsymbol{C}_{12} & 0 & 0 & 0 \\ \boldsymbol{C}_{11} & \boldsymbol{C}_{12} & \boldsymbol{C}_{11} & 0 & 0 & 0 \\ 0 & 0 & 0 & \boldsymbol{C}_{66} & 0 & 0 \\ 0 & 0 & 0 & 0 & \boldsymbol{C}_{66} & 0 \\ 0 & 0 & 0 & 0 & 0 & \boldsymbol{C}_{66} \end{bmatrix} \tag{8}$$

where $\boldsymbol{C}_l$ is rigidity matrix of the metal liner; $\boldsymbol{C}_{11}$ - $\boldsymbol{C}_{66}$ are rigidity coefficients of the metal liner.

2.3. Behaviour of the multi-layer composite

The laminate is anisotropic and the characterisation of its behaviour in cylindrical coordinate system requires to take into account orientation of the fibres (see Fig. 2). Engineer constants of this type of material are: E_x longitudinal modulus of elasticity; E_y and E_z are transverse modulus of elasticity according to y and v axis respectively; G_{xy}, G_{yv}, and G_{xv} shear modulus according to x, y, and v axis respectively; ν_{vx} and ν_{yx} are Poisson's ratios in the planes v-x and y-x respectively; γ_{xy} is shear strain in the plane x-y [14].

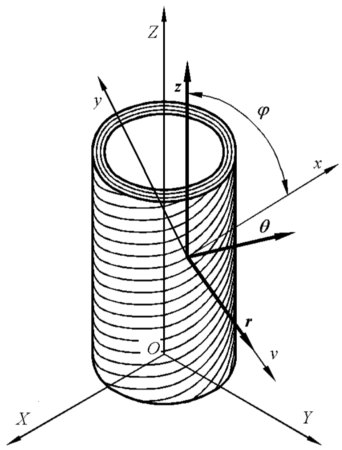

Fig. 2 Coordinate relation between cylindrical reference and the reference mark of the fibre

The distribution of fibres for unidirectional composite is similar in the directions y and z. Thus, the properties are equivalent in the plane y-v

$$E_y = E_v \tag{9a}$$

$$G_{vx} = G_{yx} \tag{9b}$$

$$\nu_{vx} = \nu_{yx} \tag{9c}$$

$$G_{vy} = \frac{E_y}{2(1+\nu_{vy})} \tag{9d}$$

where x and y are the principal axes of the longitudinal and transverse fibres respectively.

The filament winding mode permits a transverse isotropy on the reinforcement layers. The components of the matrix of rigidity are written as follows [14]

$$\boldsymbol{C} = \begin{bmatrix} \boldsymbol{C}_{11} & \boldsymbol{C}_{12} & \boldsymbol{C}_{12} & 0 & 0 & 0 \\ \boldsymbol{C}_{12} & \boldsymbol{C}_{22} & \boldsymbol{C}_{23} & 0 & 0 & 0 \\ \boldsymbol{C}_{12} & \boldsymbol{C}_{23} & \boldsymbol{C}_{22} & 0 & 0 & 0 \\ 0 & 0 & 0 & \dfrac{\boldsymbol{C}_{22}-\boldsymbol{C}_{23}}{2} & 0 & 0 \\ 0 & 0 & 0 & 0 & \boldsymbol{C}_{66} & 0 \\ 0 & 0 & 0 & 0 & 0 & \boldsymbol{C}_{66} \end{bmatrix} \tag{10}$$

where $\boldsymbol{C}$ is rigidity matrix of the composite material; $\boldsymbol{C}_{11}$ - $\boldsymbol{C}_{66}$ are rigidity coefficients of the composite material of respective layers.

The relations defined below are not general and applied in the case of rotation about z direction of the initial base. The change of base, which interested us, in this case takes place between the initial base $\boldsymbol{Q_i}(x, y, z)$ and the base of cylindrical coordinate $\boldsymbol{Q_i}(r, \theta, z)$, which can be ex pressed as

$$\begin{cases} \sigma'_{ij} = \boldsymbol{T}_\sigma\ \sigma_{ij} \\ \varepsilon'_{ij} = \boldsymbol{T}_\varepsilon\ \varepsilon_{ij} \end{cases} \tag{11a}$$

where σ'_{ij} and ε'_{ij} are stress and strain vectors expressed in the base of $\boldsymbol{Q_i}(r, \theta, z)$; σ_{ij} and ε_{ij} are stress and strain vectors expressed in the base of $\boldsymbol{Q_i}$ (x, y, z); $\boldsymbol{T}_\sigma$ and $\boldsymbol{T}_\varepsilon$ are matrixes of the base change of the stress and the strain respectively [14]. Since vectorial form of the stresses and strains, the matrices of basic changes are expressed, where φ_w is the winding angle about z .

$\boldsymbol{T}_\sigma$ and $\boldsymbol{T}_\varepsilon$ are expressed respectively as follows

$$\boldsymbol{T}_\sigma = \begin{bmatrix} cos^2\varphi & sin^2\varphi & 0 & 0 & 0 & 2\,sin\varphi\,cos\varphi \\ sin^2\varphi & cos^2\varphi & 0 & 0 & 0 & -2\,sin\varphi\,cos\varphi \\ 0 & 0 & 1 & 0 & 0 & 0 \\ 0 & 0 & 0 & cos\varphi & -sin\varphi & 0 \\ 0 & 0 & 0 & sin\varphi & cos\varphi & 0 \\ -sin\varphi\,cos\varphi & sin\varphi\,cos\varphi & 0 & 0 & 0 & cos^2\varphi - sin^2\varphi \end{bmatrix} \tag{11b}$$

$$
\boldsymbol{T}_{\varepsilon}=\begin{bmatrix} cos^2\varphi & sin^2\varphi & 0 & 0 & 0 & sin\,\varphi\, cos\,\varphi \\ sin^2\varphi & cos^2\varphi & 0 & 0 & 0 & -sin\,\varphi\, cos\,\varphi \\ 0 & 0 & 1 & 0 & 0 & 0 \\ 0 & 0 & 0 & cos\,\varphi & -sin\,\varphi & 0 \\ 0 & 0 & 0 & sin\,\varphi & cos\,\varphi & 0 \\ -2\,sin\,\varphi\, cos\,\varphi & 2\,sin\,\varphi\, cos\,\varphi & 0 & 0 & 0 & cos^2\varphi - sin^2\varphi \end{bmatrix} \tag{11c}
$$

Rigidity matrix of the composite is written in the following form [14]

$$
\boldsymbol{C}_c=\begin{bmatrix} \boldsymbol{C}_{11} & \boldsymbol{C}_{12} & \boldsymbol{C}_{13} & 0 & 0 & \boldsymbol{C}_{16} \\ \boldsymbol{C}_{12} & \boldsymbol{C}_{22} & \boldsymbol{C}_{23} & 0 & 0 & \boldsymbol{C}_{26} \\ \boldsymbol{C}_{13} & \boldsymbol{C}_{23} & \boldsymbol{C}_{33} & 0 & 0 & \boldsymbol{C}_{36} \\ 0 & 0 & 0 & \boldsymbol{C}_{44} & \boldsymbol{C}_{45} & 0 \\ 0 & 0 & 0 & \boldsymbol{C}_{45} & \boldsymbol{C}_{55} & 0 \\ \boldsymbol{C}_{16} & \boldsymbol{C}_{26} & \boldsymbol{C}_{36} & 0 & 0 & \boldsymbol{C}_{66} \end{bmatrix} \tag{12}
$$

2.4. Problem position

Substituting equation (2) in to equation (5a) and using equation (6), the following differential equation is obtained

$$
\frac{d^2U_r^{(k)}}{dr^2}+\frac{1}{r}\frac{dU_r^{(k)}}{dr}-\frac{\boldsymbol{C}_{22}^{(k)}/\boldsymbol{C}_{33}^{(k)}}{r^2}U_r^{(k)}= =\frac{\boldsymbol{C}_{12}^{(k)}-\boldsymbol{C}_{13}^{(k)}}{\boldsymbol{C}_{33}^{(k)}}\frac{\varepsilon_0}{r}+\frac{\boldsymbol{C}_{26}^{(k)}-2\boldsymbol{C}_{36}^{(k)}}{\boldsymbol{C}_{33}^{(k)}}\gamma_0 \tag{13}
$$

For an anisotropic material

$$
\boldsymbol{C}_{22}^{(k)}/\boldsymbol{C}_{33}^{(k)}>0\,;\ \boldsymbol{C}_{22}^{(k)}/\boldsymbol{C}_{33}^{(k)}\neq 1
$$

That is to say $\beta^{(k)}=\sqrt{\boldsymbol{C}_{22}^{(k)}/\boldsymbol{C}_{33}^{(k)}}$; solution of the equation (13) takes the form:

if $\beta^{(k)}=1$, then

$$
U_r^{(k)}=D^{(k)}r+J^{(k)}/r \tag{14a}
$$

if $\beta^{(k)}\neq 1$

$$
U_r^{(k)}=D^{(k)}r^{\beta^{(k)}}+J^{(k)}r^{-\beta^{(k)}}+\alpha_1^{(k)}\varepsilon_0 r+\alpha_2^{(k)}\gamma_0 r^2 \tag{14b}
$$

where

$$
\alpha_1^{(k)}=\frac{\boldsymbol{C}_{c12}^{(k)}-\boldsymbol{C}_{c13}^{(k)}}{\boldsymbol{C}_{c33}^{(k)}-\boldsymbol{C}_{c22}^{(k)}}\,,\ \alpha_2^{(k)}=\frac{\boldsymbol{C}_{c26}^{(k)}-2\boldsymbol{C}_{c36}^{(k)}}{4\boldsymbol{C}_{c33}^{(k)}-\boldsymbol{C}_{c22}^{(k)}} \tag{15}
$$

here $D^{(k)}$ and $J^{(k)}$ are integration constants.

2.5. Boundary conditions

Boundary conditions on one hand are imposed by geometry conditions of the structure, since one supposes the continuity and volume conservation and the conditions of loading on the other hand. It is supposed that there are no slips in the interfaces and that there are continuity of stresses and displacements. These boundary conditions allow determining the integration constants.

The number of unknown factors, or integration constant of the system, to be solved is $2(N+1)$ for N layers of the tube composite/liner; where $D^{(k)}$, $J^{(k)}$, γ_0, and ε_0 for $k\in[1,\,N]$.

The radii $R_{int}^{(k)}$ and $R_{ext}^{(k)}$ are introduced for each layer k and it is noted that

$$
R_{int}^{(1)}=r_0 \quad \text{and } R_{ext}(N)=r_a \tag{16}
$$

The condition of continuity of radial displacements results in the relation

$$
\forall k\in[1,\,N-1],\quad U^{(k)}\left(R_{ext}(k)\right)=U^{(k+1)}\left(R_{ext}(k)\right) \tag{17}
$$

The condition of continuity of radial stress results in

$$
\left.\begin{aligned} &\forall\, k\in[1,\,N-1],\ \sigma_r^{(k)}\left(R_{ext}(k)\right)=\sigma_r^{(k+1)}\left(R_{ext}(k)\right) \\ &\sigma_r^{(1)}\left(R_0\right)=-p_0 \\ &\sigma_r^{(N)}\left(R_{ext}(N)\right)=0 \end{aligned}\right\} \tag{18}
$$

The equilibrium condition of axial force due internal pressure with end loading effect

$$
2\pi\sum_{k=1}^{N}\int_{r_{k-1}}^{r_k}\sigma_z^{(k)}(r)\,r\,dr=\pi r_0^2\,p_0+F \tag{19}
$$

where F is the applied axial load.

Torque balance is

$$
2\pi\sum_{k=1}^{N}\int_{r_{k-1}}^{r_k}\tau_{z\theta}(r)\,r^2dr=M \tag{20}
$$

where M is the applied torque.

The hypothesis of this study neglects torque and axial loads, where $F=0$ and $M=0$. Thus one has $2(N+1)$ equations to identify the whole integration constants.

3. Algorithm of the procedure

Analytical procedure of elastic behaviour resolution of a multi-layer tube reinforced by a metal liner under pressure is solved using MATLAB software. This analysis of a comparative study enters both types of laminate: the quasi-isotropic $[\pm\varphi_n/90_{2n}]$, and anti-symmetric $[\pm\varphi_{2n}]$, where n=1. The two types of laminates are coated on a metal liner. The first type of stacking sequences $[\pm\varphi_n/90_{2n}]$ is marked as: Seq1, Seq2, and Seq3. The second type $[\pm\varphi_{2n}]$ is marked as: Seq4, Seq5, and Seq6. Table 1 presents the stacking sequences of the different studied laminates, where the order of stacking angle of each laminate is taken from interior to external. The tube is characterised by an internal radius of 50 mm, 0.5 mm thickness of the liner and as well as each layer of the composite. The properties of two materials are presented in Table 2.

Table 1

Stacking sequences of the tube under pressure

Sequence types	Angle of wrap
Seq1	Liner/[± 30/(90)$_2$]
Seq2	Liner/[± 45/(90)$_2$]
Seq3	Liner/[± 60/(90)$_2$]
Seq4	Liner/[± 30]$_2$
Seq5	Liner/[± 45]$_2$
Seq6	Liner/[± 60]$_2$

Table 2

Elastic characteristics

Properties	Carbon/epoxy (T300/934)	Liner aluminium
E_x, GPa	141.6	69.5
E_y, GPa	10.7	69.5
G_{xy}, GPa	3.88	26.7
ν_{yx}	0.268	0.3
ν_{zy}	0.495	-

Internal wall of the composite tube is subjected to internal pressure of 10 MPa. All results are represented as a function of non-dimensional ratio R, which is expressed as

$$R = \frac{r - r_0}{r_a - r_0} \tag{21}$$

where r_a is the external radius of the multi-layer tube.

4. Results and discussions

4.1. Stresses

The distribution of the stresses σ_z, σ_θ, σ_r and $\tau_{z\theta}$ along thickness is important in order to locate the critical zones. The obtained results show the presence of compression stresses on the internal wall and tension stress on the external wall of the composite tube.

4.1.1. Axial stress

The variation of axial stress σ_z for the two types of stacking sequences versus non-dimensional ratio R is shown in Fig. 3. Both types of sequences present a discontinuous variation of σ_z along thickness and the change of the fibres orientation from one layer to another influences the stress behaviour. The obtained results of stress σ_z show a large difference for the two types of stacking sequence.

The first type sequence $[\pm\varphi_n/90_{2n}]$. The variation of axial stress σ_z from the internal wall to the external one is obtained on three stages for the laminates Seq1 to Seq3 (Fig. 3): these three stages are limited from the ratio R, the first from 0 and 0.4, the second from 0.4 to 0.8, and the third from 0.8 to 1.0. No noticeable difference is in the first as well as in the third stage and the values of the stress σ_z in these stages reaches 545 and 90 MPa respectively. The second stage is characterized by big difference of σ_z values. Indeed, the stress σ_z decreses to reach 420 MPa for the laminate Seq3, however it increases to reach 930 and 710 MPa for the Seq1 and Seq2 respectively. Moreover, the second stage is characterised by the maximum stress for Seq1 and Seq3 by the minimum stress.

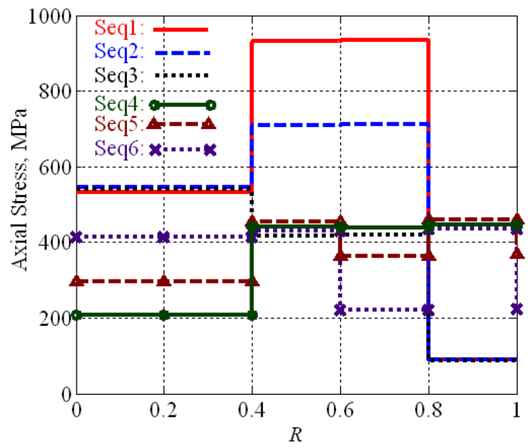

Fig. 3 Axial distribution of stress σ_z versus ratio R

The second type sequence $[\pm\varphi_{2n}]$. For the laminates Seq4, Seq5, and Seq6 axial stress σ_z versus ratio R is characterised by the stages and it is significantly lower comparatively to the first type of laminates. In the first stage (R from 0 to 0.4) the laminate Seq4 has the lowest σ_z fallowed by Seq5 and finally Seq6 having the values 207, 295 and 414 MPa respectively. However, the phenomena adverse in the stage 3 (R from 0.6 to 0.8) and the values of σ_z for the Seq4, Seq5, and Seq6 are 440, 360 and 220 MPa respectively. There is no noticeable difference of σ_z in the stage 2 (R from 0.4 to 0.6) and stage 3 (R from 0.6 to 0.8).

4.1.2. Circumferential stress

The distribution of circumferential stress σ_θ for the two types of stacking sequences versus non-dimensional ratio R is shown in Fig. 4. This distribution is in three stages for the first type of the staking and four stages in the second one. Moreover, the same remark of the discontinuous variation in Fig. 3 is recorded for this stress. The values of the stress σ_θ for the first type of stacking are much lower than for the second type in the internal wall (R=0).

The first type sequence $[\pm\varphi_n/90_{2n}]$. The variations of σ_θ are characterised by an increase from the internal wall to the external one and occur in three stages. The laminate Seq1 is characterised by the largest σ_θ followed by Seq2 and finally Seq3 in the first stage (R from 0 to 0.4) as well as in the third one (R from 0.8 to 1) reaching the maximum. However, in the second stage the phenomena are in adverse with the laminate Seq3 which has the largest stress values followed by Seq2 and finally Seq1. In addition, the minimal stress (8 MPa) is recorded for the laminate Seq3 in the first stage and the maximal one (405 Mpa) for the Seq1 in the third stage.

The second type sequence [$\pm\varphi_{2n}$]. The laminate Seq4 has the maximum stress σ_θ (240 MPa) in the internal wall, e.g. in the first stage (R from 0 to 0.4) and decreases in the second and the third but increase slightly in the forth stage. However, the laminates Seq5 and Seq6 have the minimum stresses σ_θ (300 and 270 MPa respectively) and increase to reach the maximum in the second stage. Moreover, the minimum stress of 60 MPa is obtained for the laminate Seq6 in the first stage and the maximum of 300 MPa in the second stage (R from 0.4o 0.6) of the same laminate.

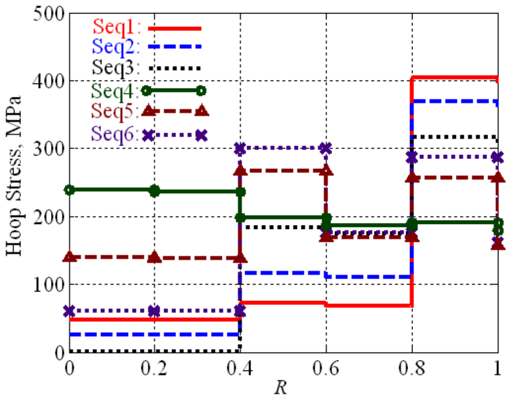

Fig. 4 Circumferential stress distribution versus ratio R

Fig. 5 shows the linear variation of stress ratio σ_θ/σ_z versus ratio R through the thickness of the composite/liner tube for the two types of stacking sequence.

The stress ratio σ_θ/σ_z has constant values versus R, and has significant values for the laminates of Seq4, Seq 5, and Seq6 [$\pm\varphi_{2n}$] types compared to these obtained for the

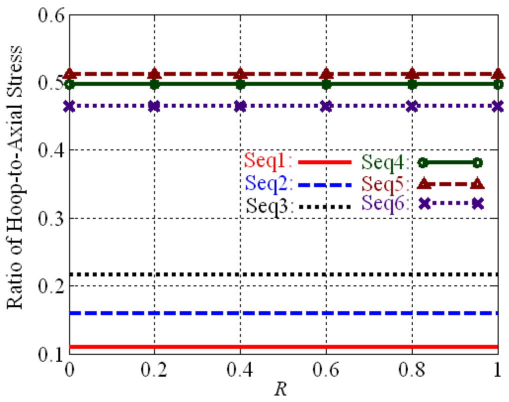

Fig. 5 Variation of the stress ratio σ_θ/σ_z along the non-dimensional R of the composite/linear tube

laminates of Seq1, Seq2 and Seq3 [$\pm\varphi_n/90_{2n}$] types. Moreover, the laminate Seq1 has the lowest values of stress ratio σ_θ/σ_z (0.11) and the laminate Seq5 has the biggest one (0.51).

4.1.3. Radial stress

The behaviour of radial stress σ_r through the tube thickness of entire composite [15] is totally different compared to the results obtained for liner/composite tube. Fig. 6 shows the distribution of radial stress σ_r through the thickness of composite/liner tubes. The behaviour of radial stress through the thickness indicates the presence of maximal compression of -10 MPa in the internal wall and minimal (equal to zero) in the external wall for all the studied laminates. In addition, this distribution of stresses from the internal wall to the external one has a linear behaviour with an increase of the slope. The curves of radial stress σ_r for the laminates of the first type [$\pm\varphi_n/90_{2n}$] (Seq1, Seq2, and Seq3) are below than the laminates of the second type [$\pm\varphi_{2n}$] (Seq4, Seq5 and Seq6), e.g. the stress σ_r is more important for the laminates of the first type than for the second ones. Indeed the Seq4 has the lowest stress σ_r and the Seq1 has the highest one.

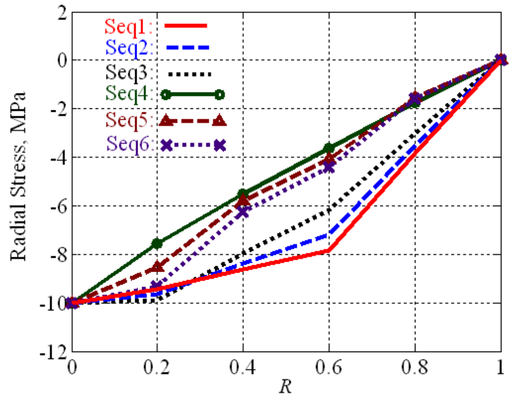

Fig. 6 Distribution of radial stress through the thickness

4.1.4. Shear stress

Discontinuous variation for the two types of stacking sequence of the shear stress $\tau_{z\theta}$ versus the ratio R is shown in Fig. 7. The variation of $\tau_{z\theta}$ from the internal wall to the external one is obtained on the four stages limiting from the ratio R, the first from 0 to 0.4, the second from 0.4 to 0.6, the third from 0.6 to 0.8, and the last one from 0.8 to 1.

The first type sequence [$\pm\varphi_n/90_{2n}$]. The stress $\tau_{z\theta}$ is zero (nearly zero -0.4 MPa) in the first stage and it reaches maximum in the second stage decreases minimum in the third one and finally becomes equal to zero in the last stage. It should be noticed that the maximum and the minimum of the stress $\tau_{z\theta}$ has the same values but one positive with indicating the presence of tension and the other negative indicating compression case. In addition the laminate Seq1 has the lowest values of the stress $\tau_{z\theta}$ falowed by Seq2 and finally Seq3 having the values of 265, 345 and 365 MPa respectively.

The second type [$\pm\varphi_{2n}$]. The same behaviour of the first type is recorded there. The stage one is characterised by positive lowest values of the stress $\tau_{z\theta}$ where the laminate Seq6 has the largest one and the laminate Seq4 has the smallest one (zero). The stress reaches the maximum in the second stage and, as well as in the first stage, the laminate Seq6 has the largest values of the stress followed by Seq5 and finally Seq4 having the values of 400, 315 and 240 MPa. In the third stage the stress $\tau_{z\theta}$ decreases and becomes negative reaching the minimum. The last stage is the same as the second one. In addition the laminate Seq4 has the lowest values of the stress $\tau_{z\theta}$ in the thickness for all the stages.

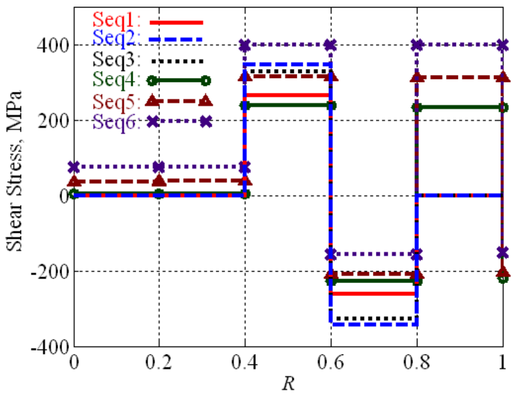

Fig. 7 Distribution of the shear stress in the thickness according to ratio R

4.2. Strains

Axial, radial, and circumferential variations of strains in the thickness of composite/liner tube for the two types of staking sequence are represented respectively in Figs. 8, 9, and 10. It is noticed that positive strains indicate the presence of a tension state and the negative ones show the presence of a compression case.

Axial strain in the thickness is constant and the laminates Seq1 Seq2 and Seq3 of the $[\pm\varphi_n/90_{2n}]$ type have the greatest values. They are closer comparatively to the laminates Seq4, Seq5, and Seq6 $[\pm\varphi_{2n}]$ type. The laminate Seq4 has the lowest axial stress and Seq2 has the greatest one (Fig. 8).

The variation of radial strain in thickness is linear and occurs in three stages (Fig. 9) for all studied laminates. Radial strain is constant in the first stage (R from 0 to 0.2) and decreases sharply and becomes negative in the second stage (R from 0.2 to 0.4) and finally increases slightly in

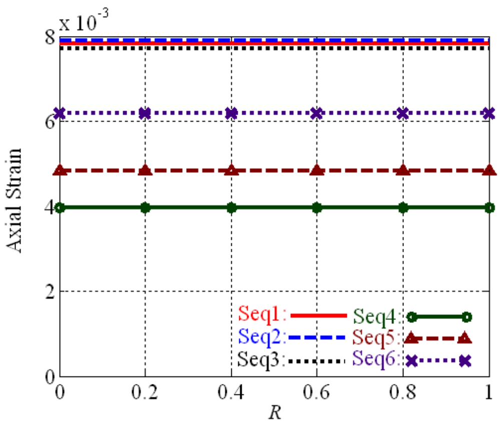

Fig. 8 Axial strain variations in thickness

the last stage (R from 0.4 to 1). It should be noticed that the laminates of $[\pm\varphi_n/90_{2n}]$ type have the greater values of radial strain in tension and in compression than $[\pm\varphi_{2n}]$.

Linear behaviour occurs in two stages for the variations of circumferential strain in thickness (Fig. 10). The decrease is very weak in the first stage (R from 0 to 0.2) for the circumferential strain and it becomes more significant in the second stage (R from 0.2 to 1). The laminate Seq4 has the greatest values of the circumferential strain and Seq3 has the lowest one. In addition Seq2 and Seq6 are really too close.

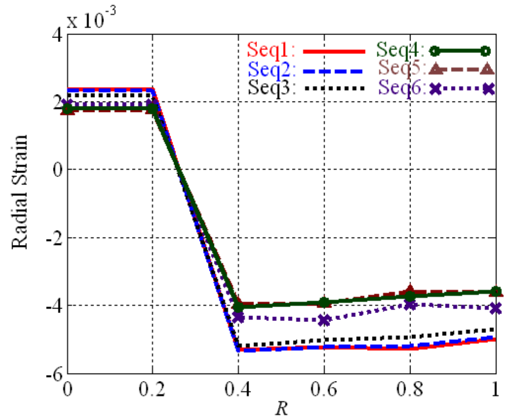

Fig. 9 Radial strain variations in thickness

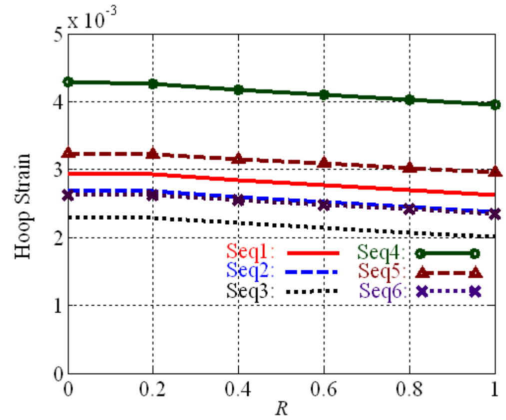

Fig. 10 Circumferential strain variations in thickness

4.3. Displacements

Fig. 11 shows the variation of radial displacements for the two laminate types of stacking sequence studies. The analysis of these results is exactly similar to the variations of the circumferential strain through the thickness (Fig. 10).

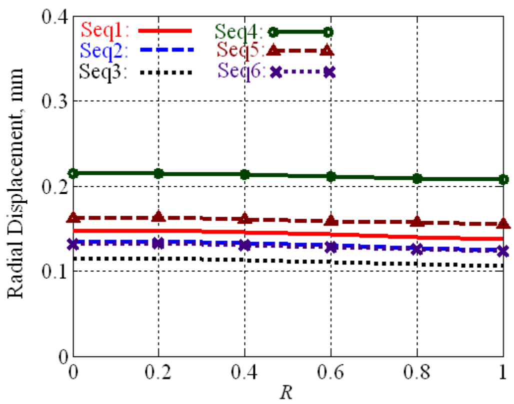

Fig. 11 Radial displacement variations in thickness

5. Conclusions

The study presents an elastic analytical modelling of a multilayer composite cylindrical tank coated on an aluminium liner for two types of stacking: multilayer antisymmetric $[\pm\varphi_{2n}]$ and quasi-isotropic laminate $[\pm\varphi_n/90_{2n}]$. An analysis of the distribution of stress, displacement, and deformations are discussed there. The variation of all the discussed parameters are represented through the thickness of the composite tube and according to a non-dimensional ratio R. The analysis of the obtained results makes it possible to release that:

- the laminate Seq3 liner/[±60/(90)$_2$] for stacking sequence [$\pm\varphi_n/90_{2n}$] has the best results, in terms of stresses and displacements comparatively to the two other laminates Seq1 and Seq2. The same remark is recorded for Seq6 liner/[(±60)$_2$] comparatively to Seq6 and Seq5 for the staking sequence [$\pm\varphi_{2n}$];
- the stress ratio σ_θ/σ_z is constant and it varies from a sequence to another according to the angle of orientation of each layer. In this investigation the stress ratio indicates that axial stresses are much more important than circumferential ones;
- the metal liner produces a remarkable fall of stresses and displacements, although it accounts for 1/5 of the total thickness of the tank;
- the assumption of heating effects responsibility is essential. This point will be the future object of the works. A thermo mechanical comparative study enters quasi-isotropic liner/[(±60)/(90)$_2$] and the anti-symmetrical liner/[(±60)$_2$] will be established.

6. References

1. **Bezazi, A.**, **El Mahi, A.**, **Berthelot, J.-M.**, **Bezzazi, B.** Flexural fatigue behaviour of cross-ply laminates -An experimental approach. -Strength of Materials, 2003, v.35, No2, p.149-161.
2. **Bezazi, A.**, **El Mahi, A.**, **Berthelot, J.-M.**, **Bezzazi, B.** Analyse de l’endommagement des stratifiés en flexion 3-points. Influence de la séquence d’empilement. XV^{ème} Congrès Français de Mécanique, Nancy, 2001, p.[1-6]
3. **Liang, C.C.**, **Chen, H.W.** and **Wang, C.H.** Optimum design of dome contour for filament-wound composite pressure vessels based on a shape factor. -Composite Structure, 2002, v.58, p.469-482.
4. **Verijenco, V.E.**, **Adali, S.**, **Tabakov, Y.P.** Stress distribution in continuously heterogeneous thick laminated pressure vessels. -Composite Structures, 2001, v.54, p.371-377.
5. **Vasiliev, VV.**, **Krinakov, A.A.**, **Razin, A.F.** New generation of filament-wound composite pressure vessels for commercial applications. -Composite Structure, 2003, v.62, p.449-459.
6. **Wild, P.M.** Analysis of filament-wound cylindrical shells under combined centrifugal, pressure and axial loading. -Composites, Part A, 1997, v.28 A, p.47-55.
7. **Lifshitz, J.M.**, **Dayan, H.** Filament–wound pressure vessel with thick metal liner. -Composite Structures, 1995, v.32, p.313-323.
8. **Hocine, A.**, **Bezazi, A.**, **Benamar, A.** Analysis of the influence of stacking sequence on the mechanical behaviour of composite fuel tanks.-JNC14 -2005, Compiègne, Published by Benzaggah M.L. and Lamon J., p.641-649.
9. **Rosenow, M.W.K.** Wind angle effects in glass fiber-reinforced polyster filament wound pipes. -Composites, 1984, v.15, p.144-52.
10. **Xia**, **M.**, **Takayanagi, H.**, **Kemmochi, K.** Analysis of multi-layered filament -wound composite pipes under internal pressure. -Composites Structures, 2001, v.53, p.483-491.
11. **Xia**, **M.**, **Takayanagi, H.**, **Kemmochi, K.** Analysis of filament-wound reinforced sandwich pipe under combined internal pressure and thermomechanical loading. Composite Structures, 2001, v.51, p.273-283.
12. **Germain, P, Muller, P.** Introduction à la mécanique des milieux continus. -Paris, Milan, Barcelone: Masson, 1995.-467p.
13. **Timoshenko S., Woinowsky-Krieger S.** Theory of Plates and Shells.-New York: McGraw-Hill Book Company, Inc., 1959.-580p.
14. **Berthelot, J.-M.** Composite Materials. Mechanical Behavior and Structural Analysis.-New York: Springer, 1999.-676p.
15. **Hocine, A.**, **Boubakar, L**., **Bezazi, A.**, **Benamar, A.** Analyse d’un réservoir multicouche de stockage d’hydrogène.-Workshop sur l’hydrogène WIH2’2005 - CDER, Alger 2005, p.[1-8].

A. Hocine, A. Bezazi, L. Boubakar, A. Benamar, A. Kondratas

DAUGIASLUOKSNIS VAMZDINIS KOMPOZITAS SU ĮKLOTU: ELGSENOS, VEIKIANT SLĖGIUI, MODELIAVIMAS

R e z i u m ė

Darbe pateikta daugiasluoksnio vamzdžio (t. y. cilindrinio bako vidurinės dalies), armuoto metaliniu įklotu, įtempimų ir deformacijų, veikiant vidiniam ir išoriniam slėgiui, analizė. Tamprios struktūros elgsenai analizuoti buvo taikomas analitinis modeliavimo metodas. Darbo tikslas buvo ištirti atitinkamą kompozito sluoksnių sudarymo eiliškumą, kad būtų galima padidinti bako atsparumą didesniems slėgiams. Buvo modeliuoti du kompozito sluoksnių sudarymo ant įkloto eiliškumo tipai: antisimetrinis ir kvaziizotropinis. Ištirti cilindrinio bako vidurinės dalies ašiniai, apskritiminiai, radialiniai ir šlyties įtempiai bei deformacijos tomis pačiomis kryptimis ir įtempių santykis bako sienelės storio atžvilgiu. Be to, buvo tirtas parametrų kitimas bako sienelės storio, išreikšto santykine radialine koordinate, atžvilgiu. Gauti rezultatai parodė, kad anksčiau minėti parametrai kinta priklausomai nuo kompozitų sluoksnių sudarymo ant įkloto eiliškumo ir nuo sluoksnių pluoštų orientacijos.

A. Hocine, A. Bezazi, L. Boubakar, A. Benamar, A. Kondratas

MULTILAYER TUBULAR COMPOSITE REINFORCED BY A LINER: BEHAVIOUR UNDER PRESSURE LOADING SIMULATION

S u m m a r y

This paper presents an analysis of stresses and strains of a multi-layer composite tube (tubular part of the cylindrical tank) reinforced by a metal liner under an internal and external pressure loadings. The analytical procedure of simulation is used for the investigation of the elastic behavior of the structure under pressure. The aim of this study is to determine the adequate stacking sequence in order to improve the resistance of the tank to support higher pressures. In this simulation two types of coated on a metal liner laminates stacking sequences are used: the anti-symmetric stacking and the quasi-isotropic. The axial, circumferential, and radial stresses and strains as well as stress ratio and shear stress in relation to the thickness of the tube walls were investigated. Moreover, the variations of the mentioned parameters are investigated in relation to the thickness of the composite tube expressed as non-dimensional radial coordinate. The obtained results show that the mentioned parameters vary depending on the stacking sequence and according to the orientation angle of each fibre layer.

А. Хоцине, А. Безази, Л. Боубакар, А. Бэнамар, А. Кондратас

МНОГОСЛОЙНЫЙ ТРУБЧАТЫЙ КОМПОЗИТ УСИЛЕННЫЙ ВКЛАДЫШЕМ: МОДЕЛИРОВАНИЕ ПОВЕДЕНИЯ ПОД НАГРУЗКОЙ ДАВЛЕНИЕМ

Р е з ю м е

В работе представлен анализ напряжений и деформаций многослойного трубчатого композита (трубчатой части цилиндрического бака), усиленного металлическим вкладышем под нагрузкой внутреннего и внешнего давления. Для анализа упругого поведения структуры под давлением использован аналитический метод моделирования. Целью этого исследования является определение соответствующей последовательности нанесения слоев композита, чтобы увеличить способность бака выдерживать более высокие давления. Для моделирования применены два типа нанесения слоев на металлический вкладыш: антисимметричный и квазиизотропный. Исследованы осевые, окружные и радиальные напряжения и деформации трубчатой части цилиндрического бака, а также напряжения сдвига и соотношение напряжений относительно толщины стенки бака. Кроме того, исследованы изменения упомянутых параметров относительно толщины стенки композита, выраженной как относительная радиальная координата. Полученные результаты показывают, что упомянутые параметры изменяются в зависимости от последовательности нанесения слоев на металлический вкладыш, а также от угла ориентации волокон каждого слоя.

Received April 15, 2005